The Astrophysical Journal, 689:1150–1160, 2008 December 20

GeV EMISSION FROM PROMPT AND AFTERGLOW PHASES OF GAMMA-RAY BURSTS

Shin'ichiro Ando, Ehud Nakar, and Re'em Sari
California Institute of Technology, Mail Code 130-33, Pasadena, CA 91125;
ando@tapir.caltech.edu, udini@tapir.caltech.edu, sari@tapir.caltech.edu
Received 2007 August 6; accepted 2008 August 11

ABSTRACT

We investigate the GeV emission from gamma-ray bursts (GRBs) using the results from the Energetic Gamma Ray Experimental Telescope (EGRET) and in view of the *Gamma-Ray Large Area Space Telescope* (*GLAST*). Assuming that the conventional prompt and afterglow photons originate from synchrotron radiation, we compare an accompanying inverse-Compton component with EGRET measurements and upper limits on GeV fluence, taking Klein-Nishina feedback into account. We find that the EGRET constraints are consistent with the theoretical framework of the synchrotron self-Compton model for both prompt and afterglow phases, and discuss constraints on microphysical parameters in both phases. Based on the inverse-Compton model and using EGRET results, we predict that *GLAST* would detect GRBs with GeV photons at a rate of $\gtrsim 20\ \mathrm{yr}^{-1}$ from both the prompt and afterglow phases. This rate applies to the high-energy tail of the prompt synchrotron emission and to the inverse-Compton component of the afterglow. Theory predicts that in a large fraction of the cases where synchrotron GeV prompt emission would be detected by *GLAST*, inverse-Compton photons should also be detected at high energies ($\gtrsim$10 GeV). Therefore, *GLAST* will enable a more precise test of the high-energy emission mechanism. Finally, we show that the contribution of GRBs to the flux of the extragalactic gamma-ray background measured with EGRET is at least 0.01%, and likely around 0.1%.

Subject headings: gamma rays: bursts — radiation mechanisms: nonthermal

Online material: color figures

1. INTRODUCTION

Cosmological gamma-ray bursts (GRBs) have released a tremendous amount of energy in the past and present universe. Their emission covers a very wide range of frequencies: a highly variable prompt phase radiates ~100 keV gamma rays, while a subsequent afterglow radiates radio to X-ray photons. It is likely that the bulk of these photons are emitted by gyration of relativistic electrons in magnetic fields, e.g., by synchrotron radiation. The relativistic electrons are accelerated either by internal dissipation (for prompt emission) or by external shocks (for afterglows). For reviews, see Piran (2005), Mészáros (2006), and Nakar (2007).

GeV photons were also detected from several GRBs by the Energetic Gamma Ray Experimental Telescope (EGRET) on board the *Compton Gamma-Ray Observatory* (*CGRO*) (Schneid et al. 1992, 1995; Sommer et al. 1994; Hurley et al. 1994; González Sánchez et al. 2003). The data are still not sufficient for us to firmly infer the emission mechanisms of these GeV gamma rays, but the most promising mechanism is synchrotron self-Compton (SSC) scattering (e.g., Mészáros et al. 1994; Waxman 1997; Wei & Lu 1998; Chiang & Dermer 1999; Panaitescu & Kumar 2000; Zhang & Mészáros 2001; Sari & Esin 2001; Guetta & Granot 2003). This is because the relevant emission parameters, such as the energy fraction of the GRB jets going to electrons (ϵ_e) and magnetic fields (ϵ_B), are relatively well measured from the afterglow spectra and light curves; the typical values are $\epsilon_e = 0.1$ and $\epsilon_B = 0.01$ (e.g., Panaitescu & Kumar 2001; Yost et al. 2003). For prompt emission, ϵ_e is similar or even higher, as evident from the high efficiency of this phase, while ϵ_B is not well constrained. Thus, there should be a significant inverse-Compton (IC) component accompanying the synchrotron radiation in both the afterglow and prompt emission. The luminosities of the synchrotron and IC are expected to be comparable, as the IC-to-synchrotron luminosity ratio is roughly given by $(\epsilon_e/\epsilon_B)^{1/2}$, according to theory (e.g., Sari & Esin 2001).

In this paper, we explore the GeV gamma-ray emission of GRBs in the context of the SSC mechanism.[1] Besides the several GRBs detected by EGRET, there are many others for which upper bounds on the fluence were obtained (González Sánchez 2005). These ~100 GRBs should also be compared with the predictions of the SSC model, because the fluence upper limits in the EGRET energy band are comparable to the fluence of prompt emission collected by the Burst and Transient Source Experiment (BATSE) instrument on board *CGRO*. As the experimental bound is already strong, while theoretical models of the SSC process predict a large fluence for the EGRET energy range, we derive meaningful constraints from EGRET data analysis on the physics of the high-energy emission mechanisms of GRBs. This approach is different from (and therefore complementary to) that in previous studies (e.g., Dermer et al. 2000; Asano & Inoue 2007; Ioka et al. 2007; Gou & Mészáros 2007; Fan et al. 2008; Murase & Ioka 2008; Panaitescu 2008 and references therein), where the prediction of gamma-ray flux relies only on theoretical models and sub-GeV observations. We instead use EGRET data in order to infer the GeV emission and constrain the theoretical models.

We use our results to predict the expected number of GRBs that would be detected by the *Gamma-Ray Large Area Space Telescope* (*GLAST*).[2] The *GLAST* satellite is equipped with the Large Area Telescope (LAT), which is an upgraded version of EGRET. Since revealing the high-energy emission mechanisms of GRBs is one of the important objectives of *GLAST*, our prediction should give a useful guideline. Finally, we apply our results to estimate the contribution of GRBs to the diffuse extragalactic gamma-ray

[1] Our analysis and conclusions are also applicable if the MeV and/or radio-X-ray afterglow emission mechanism is not synchrotron but another type of emission from relativistic electrons that gyrate in a magnetic field, such as jitter radiation (Medvedev 2000).

[2] Since the time of writing, *GLAST* has been renamed as the *Fermi Gamma-Ray Space Telescope*.

background (EGB), which was also measured by EGRET (Sreekumar et al. 1998; Strong et al. 2004; however, see Keshet et al. 2004 for a subtle issue of Galactic foreground subtraction).

This paper is organized as follows. In § 2, we summarize the predictions of the SSC model for the prompt (§ 2.1) and afterglow (§ 2.2) phases. Section 3 is devoted to analysis of the GRB fluence data by EGRET, from which distributions of fluence in the GeV band are derived. We then use these distributions to argue prospects for GRB detection with *GLAST* in § 4, and implications for EGB from GRB emissions in § 5. In § 6, we give a summary of the paper.

2. INVERSE-COMPTON MODEL OF HIGH-ENERGY EMISSION

If the prompt and/or afterglow emission is due to synchrotron radiation from relativistic electrons (with Lorentz factor γ_e), then there must be an accompanying IC component from the same electrons scattering off the synchrotron photons. The spectral shape of the IC emission is almost the same as the synchrotron radiation (shifted by γ_e^2), and is expected to fall around the GeV range during both the prompt and afterglow phases. For $\epsilon_e > \epsilon_B$, and assuming that there is no "Klein-Nishina suppression" and that the emitting electrons are fast cooling, the IC fluence is related to the synchrotron fluence simply through $F_{\rm IC} \approx (\epsilon_e/\epsilon_B)^{1/2} F_{\rm syn}$. Thus, assuming that the microphysics do not vary much from burst to burst, it is natural to assume proportionality between the synchrotron MeV fluence (observed by BATSE) and the GeV synchrotron-plus-IC fluence (observed by EGRET and in the future by *GLAST*):

$$F_{\rm GeV} = (\eta_{\rm syn} + \eta_{\rm IC}) F_{\rm MeV}, \tag{1}$$

where $\eta_{\rm syn}$ and $\eta_{\rm IC}$ are coefficients for the proportionality due to the synchrotron and IC processes. Note that the synchrotron fluence in the GeV range can be extrapolated relatively easily if we assume that the spectrum extends up to such high energies. Thus, we focus here on a theoretical evaluation of the IC component. At a first approximation, the coefficient $\eta_{\rm IC}$ is roughly $(\epsilon_e/\epsilon_B)^{1/2}$ from considerations above, and thus we define

$$\eta_{\rm IC} = \left(\frac{\epsilon_e}{\epsilon_B}\right)^{1/2} \xi_{\rm KN} \xi_w \frac{F_{\rm syn}}{F_{\rm MeV}}, \tag{2}$$

where for the prompt emission $F_{\rm syn} \approx F_{\rm MeV}$, while for the afterglow $F_{\rm syn}$ is the afterglow fluence within the radio to X-ray energy bands. Correction factors $\xi_{\rm KN}$ and ξ_w represent the effects of Klein-Nishina suppression and the detector energy window, respectively; these are given below.

We define typical frequencies for both synchrotron ($\nu_{\rm syn}$) and IC ($\nu_{\rm IC}$) as the frequencies where most of the energies are radiated in cases where the Klein-Nishina cross section does not play an important role; i.e., where νf_ν for each component is peaked. From relativistic kinematics, these two typical frequencies are related through

$$\nu_{\rm IC} \approx \gamma_m^2 \nu_{\rm syn}, \tag{3}$$

where γ_m is a characteristic Lorentz factor of the electrons that dominate the synchrotron power (Rybicki & Lightman 1979); this is true in the fast-cooling regime, which is the case in most of our discussions (Sari & Esin 2001). The Klein-Nishina effect is relevant if photon energy in the electron rest frame exceeds the electron rest-mass energy, and this condition is formulated as

$$h\nu_{\rm KN} = \Gamma_b \gamma_m m_e c^2, \tag{4}$$

where Γ_b is the bulk Lorentz factor of the ejecta, which is on the order of 100 in the prompt phase of GRBs and their early afterglows. Upscattering of synchrotron photons to energies above $h\nu_{\rm KN}$ is highly suppressed, which results in an IC cutoff at $\nu_{\rm KN}$.

Besides producing a spectral cutoff, the Klein-Nishina effect also modifies the way electrons cool, which is relevant for the GeV emission and is also included in $\xi_{\rm KN}$. Electrons with energies above the Klein-Nishina threshold (for a given seed-photon energy) can lose their energies only through synchrotron radiation, while the lower energy ones can cool through both processes. Such an effect has been studied in the case where the seed photons for IC scattering are provided by an external source (e.g., Moderski et al. 2005a, 2005b and references therein). However, in the case of the SSC mechanism, since the seed photons are emitted from a synchrotron process due to the same electron population, we should take feedback into account. Giving full details on this is beyond the scope of the present paper, but some results are summarized briefly in Appendix A (see also Derishev et al. 2003). Here, we only show the approximate analytic form of $\xi_{\rm KN}$:

$$\xi_{\rm KN} \approx \begin{cases} 1 & \text{for } \gamma_m \le \gamma_{\rm KN}, \\ \left(\dfrac{\gamma_m}{\gamma_{\rm KN}}\right)^{-1/2} & \text{for } \gamma_m > \gamma_{\rm KN}, \end{cases} \tag{5}$$

where $\gamma_{\rm KN}$ is the Lorentz factor of electrons for which photons at $\nu \gtrsim \nu_{\rm syn}$ are in the Klein-Nishina regime. The energy of an observed photon with frequency ν as measured in the rest frame of an electron with Lorentz factor γ is $\approx \gamma h\nu/\Gamma_b$, where the $1/\Gamma_b$ factor converts the photon energy from the observer's frame to the plasma rest frame, and the γ factor converts it to the electron rest frame. Since such a photon is in the Klein-Nishina regime of an electron with Lorentz factor γ once its energy in the electron rest frame is larger than $m_e c^2$, we obtain

$$\gamma_{\rm KN} = \frac{\Gamma_b m_e c^2}{h\nu_{\rm syn}}. \tag{6}$$

This Klein-Nishina feedback effect modifies the spectrum shape of both synchrotron and IC emissions (in addition to the Klein-Nishina cutoff for IC). We note that equation (5) provides a solution that agrees within a factor of $\sim$2 with the one obtained by numerically solving equation (A1). This precision is sufficiently good for our purpose, especially because it is well within the uncertainty ranges of other parameters.

With ξ_w, we take into account the fraction of the IC fluence that falls into the GeV detector energy bands. The EGRET window is between $h\nu_{w,l} = 30$ MeV and $h\nu_{w,u} = 30$ GeV, while the *GLAST* LAT window is between $h\nu_{w,l} = 20$ MeV and $h\nu_{w,u} = 300$ GeV. We assume here that the frequency where most of the IC energy is released, $\nu_{\rm IC,peak} \equiv \min[\nu_{\rm IC}, \nu_{\rm KN}]$, is always larger than the lower limit of the frequency band $\nu_{w,l}$, as expected for both EGRET and *GLAST*, and thus consider the cases in which $\nu_{\rm IC,peak}$ is within or above the detector frequency band. For the case where $\nu_{w,l} < \nu_{\rm IC,peak} < \nu_{w,u}$, we have $\xi_w \approx 1$. On the other hand, if $\nu_{\rm IC,peak} > \nu_{w,u}$, then most of the energy comes from the upper frequency limit $\nu_{w,u}$, and we have $\xi_w \approx (\nu_{w,u}/\nu_{\rm IC,peak})^{2-\alpha_1}$,

where α_1 is the photon spectral index below peak frequency. Thus, we may approximate ξ_w as

$$\xi_w \approx \left(1+\frac{\min[\nu_{\rm IC},\nu_{\rm KN}]}{\nu_{w,u}}\right)^{\alpha_1-2} = \begin{cases} \left(1+\dfrac{\gamma_m^2\nu_{\rm syn}}{\nu_{w,u}}\right)^{\alpha_1-2} & \text{for } \gamma_m \le \gamma_{\rm KN}, \\ \left(1+\dfrac{\Gamma_b\gamma_m m_e c^2}{h\nu_{w,u}}\right)^{\alpha_1-2} & \text{for } \gamma_m > \gamma_{\rm KN}, \end{cases} \quad (7)$$

where $\nu_{\rm IC}/\nu_{\rm KN} = \gamma_m/\gamma_{\rm KN}$, as one can easily show.

The above discussion assumes that the density of the synchrotron photon field is proportional to the instantaneous synchrotron emissivity. In the case of a relativistically expanding radiation front, this assumption is valid when the duration over which the emissivity varies significantly (δt) is comparable to the time that has passed since the expanding shell was ejected (t_0). In this case, the ratio between the synchrotron emissivity and the synchrotron photon field density is in a steady state. When $\delta t \ll t_0$, the synchrotron photon field density may be significantly lower than in the steady state case (Granot et al. 2008), thereby suppressing the IC component. The exact suppression factor depends on the detailed spatial and temporal history of the emissivity. Theoretically, in the afterglow phase we expect $\delta t \sim t_0$. In the prompt emission phase as well, internal shock models generally predict $\delta t \sim t_0$ (Piran 1999 and references therein). Thus, in the internal-external shock model, corrections to the IC component due to this effect are expected to be on the order of unity. Therefore, in the present paper, we assume that such an effect can be neglected, and that the synchrotron photon field is proportional to the instantaneous synchrotron emissivity. One should keep in mind, however, that $\delta t \ll t_0$ is a viable possibility (see, e.g., Pe'er & Waxman 2004, 2005 for a more detailed study in such cases), especially in the highly variable prompt phase. In principle, detailed *GLAST* observations of IC emission may be able to constrain $\delta t/t_0$ during the prompt phase.

In addition, toward the higher end of the EGRET or *GLAST* energy band, photons may start to be subject to absorption due to pair creation in the source or during propagation (e.g., Baring & Harding 1997; Lithwick & Sari 2001; Razzaque et al. 2004; Ando 2004; Casanova et al. 2007; Murase et al. 2007). Although such a mechanism might be relevant for the IC yields (especially in the prompt phase) depending on some parameters that are not well constrained yet, we assume that this is not the case in the present paper. It is hoped that *GLAST* will provide information that will enable a better understanding of this issue.

2.1. *Prompt Phase*

BATSE (as well as the *Swift* satellite) has detected a large number of GRBs in the prompt phase, with gamma rays in the energy band of 20 keV–1 MeV. The spectrum is well described by a smoothly broken power law with a typical lower energy index of $\alpha_1 \approx 1$ and a higher energy index of $\alpha_2 \approx 2.3$; the spectral break typically occurs around $h\nu_{\rm syn} \approx 300$ keV, where the energy of the prompt emission νf_ν peaks (Band et al. 1993; Preece et al. 2000; Kaneko et al. 2006). As we show in Figure 1, the distribution of the fluence integrated over the BATSE energy band follows a lognormal function.[3] The peak of this distribution is $\overline{F}_{\rm BATSE} = 2.5\times10^{-6}$ erg cm^{-2}, and its standard deviation is $\sigma_{\log F} = 0.75$. The average of the BATSE fluence is therefore $\langle F_{\rm BATSE}\rangle = 10^{-5}$ erg cm^{-2}.

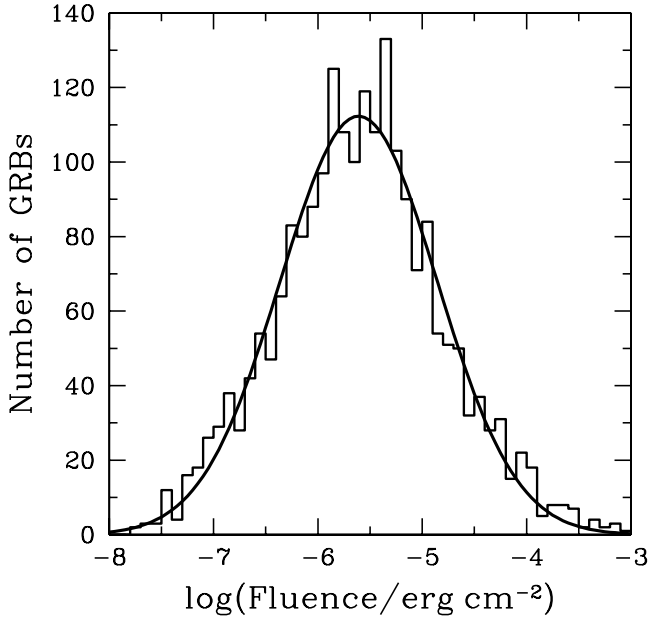

FIG. 1.—Fluence distribution in the prompt phase of BATSE GRBs. The best-fit lognormal function is also shown, where the peak is at $\overline{F}_{\rm BATSE} = 2.5\times10^{-6}$ erg cm^{-2}, and the standard deviation is $\sigma_{\log F} = 0.75$.

Therefore, for the prompt emission phase, using $\alpha_1 = 1$, $\alpha_2 = 2.3$, and $h\nu_{\rm syn} = 300$ keV, we find that

$$\gamma_{\rm KN} = 170\Gamma_{b,2}, \quad (8)$$

where $\Gamma_{b,2} = \Gamma_b/10^2$. In addition, for ξ_w, considering the *GLAST* LAT energy window (20 MeV–300 GeV) in equation (7), we obtain

$$\xi_w = \begin{cases} \left[1+\left(\dfrac{\gamma_m}{10^3}\right)^2\right]^{-1} & \text{for } \gamma_m \le 170\Gamma_{b,2}, \\ \left(1+\dfrac{\Gamma_{b,2}\gamma_m}{5900}\right)^{-1} & \text{for } \gamma_m > 170\Gamma_{b,2}. \end{cases} \quad (9)$$

Now, assuming that all electrons are accelerated in shocks, the typical value for the Lorentz factor of the relativistic electrons is given as

$$\gamma_m \approx \epsilon_e\frac{m_p}{m_e}(\Gamma_{\rm rel}-1) = 200\epsilon_{e,-1}(\Gamma_{\rm rel}-1), \quad (10)$$

where $\Gamma_{\rm rel}$ is the relative Lorentz factor of the colliding ejecta portions, and $\epsilon_{e,-1} = \epsilon_e/10^{-1}$. In the internal shock model for the prompt emission, $\Gamma_{\rm rel}-1$ is of order unity. If we adopt $\Gamma_{\rm rel} = 3$ and $\epsilon_e = 0.1$, we obtain $\gamma_m \approx 400$. Furthermore, assuming $\Gamma_b = 100$, equation (9) gives $\xi_w \approx 0.9$, and equations (5) and (8) give $\xi_{\rm KN} \approx 0.7$. By substituting these values and assuming $\epsilon_B = 0.01$ in equation (2), we obtain $\eta_{\rm IC} \approx 1.9$, which implies that under the most straightforward assumptions, a comparable fluence is expected in both the *GLAST* LAT and BATSE windows. In this case, the Klein-Nishina cutoff energy is in the *GLAST* LAT band as well as in the EGRET band ($h\nu_{\rm KN} \lesssim 30$ GeV), and thus we also obtain another comparable value of $\eta_{\rm IC} \approx 1.2$ in the EGRET case.

Note that in the case of prompt emission, the synchrotron spectrum is not negligible in the EGRET and *GLAST* LAT energy

[3] See http://www.batse.msfc.nasa.gov/batse/grb/.

bands. For canonical parameters ($h\nu_{\rm syn} = 300$ keV, $\alpha_1 = 1$, and $\alpha_2 = 2.3$), the ratio $\nu f_{\nu,{\rm IC}}/\nu f_{\nu,{\rm syn}}$ at 100 MeV is about $0.01(\epsilon_e/\epsilon_B)^{1/2}(\gamma_m/400)^{-2}$, assuming that the synchrotron spectrum continues into the GeV window without a break, and that IC is not much suppressed by the Klein-Nishina effect. Therefore, the synchrotron component dominates around the lower energy limit, where most of the photons (although not most of the fluence) are observed. In the case of EGRET, since only a handful of photons were detected in all EGRET events, these are expected to be dominated by the synchrotron low-energy ($\sim$100 MeV) photons. This indicates that the quantity we can constrain using the EGRET fluence upper limits is not $\eta_{\rm IC}$ but $\eta_{\rm syn} = F_{\rm syn}(100\ {\rm MeV})/F_{\rm MeV}$, the ratio of synchrotron fluence around 100 MeV and that in the MeV range. In addition, this picture is indeed consistent with the fact that the spectral index of GeV photons for several GRBs measured with EGRET is $\alpha = 2$–3 (e.g., Schneid et al. 1992; Sommer et al. 1994; Hurley et al. 1994). Note, however, that the *energy fluence* in the *GLAST* LAT and EGRET bands can be dominated by a much harder IC component ($\alpha \approx 1$–2) that peaks above $\sim$1 GeV and may carry up to $\sim$10 times more energy than the one observed at 100 MeV without being detected. This is because even when the $\sim$10 GeV fluence is 10 times larger, the small photon number at such high energies is still small enough to avoid detection. Thus, EGRET observations, which are consistent with measurement of the synchrotron high-energy tail, can only put an upper limit on $\eta_{\rm IC}$.

2.2. *Afterglow Phase*

The afterglow is considered to be a synchrotron emission from electrons accelerated in the external shock, which is caused by the interaction between the relativistic ejecta and the interstellar medium. In this model, the synchrotron emission dominates the spectrum from radio to X-ray. The associated IC emission is expected to dominate the GeV energy range (i.e., $\eta_{\rm IC} \gg \eta_{\rm syn}$), since the electron Lorentz factor is much larger than in the case of prompt emission (see eq. [10], where the relative and bulk Lorentz factors are the same; $\Gamma_{\rm rel} = \Gamma_b$), compensating for the smaller $\nu_{\rm syn}$ (eq. [3]). During the first several minutes (observer time), electrons might be cooling fast ($\alpha_1 = 1.5$), with $h\nu_{\rm syn} \approx 1$ keV, while $\gamma_m \approx 10^4$–10^5. This implies that the fraction of the IC energy that falls in the *GLAST* LAT energy window is close to unity; i.e., $\xi_w \approx 0.2$–0.9 from equation (7) (for EGRET $\eta_w \approx 0.08$–0.5) and $\xi_{\rm KN} \approx 0.7$–1 from equations (5)–(6). Since $h\nu_{\rm IC}$ at early times is close to the upper limit of the energy window, the effective photon index of the IC emission within the detector window during this time is $\approx$1.5–2.

At later times, the electrons are in the slow-cooling regime, and $\nu_{\rm syn}$ is the cooling frequency, while a typical γ_e is the Lorentz factor of electrons that cooled significantly (e.g., Sari & Esin 2001). In this regime, the SSC peak is very broad, and its location is almost constant with time. For typical parameters, the Klein-Nishina effect does not play a major role while the peak of the SSC emission falls within the *GLAST* LAT and EGRET windows. Therefore, at later times, $\xi_w \approx 1$ and the effective photon index within the energy windows of these detectors is $\approx$2.

One should, however, note that on long timescales the GeV background becomes important, making it hard to detect the GeV afterglow. Therefore, the optimal timescale for a GeV afterglow search would be $\sim$100–1000 s (Zhang & Mészáros 2001). The afterglow GeV fluence, $F_{\rm GeV}$ in equation (1), is that integrated over a given timescale, while $F_{\rm MeV}$ is collected over roughly T_{90}, during which 90% of the MeV photons are counted. The total energy radiated away by the radio to X-ray afterglow during every decade is roughly 1%–10% of the energy emitted in the prompt phase. Therefore, we expect a bright GeV afterglow that radiates about 0.01–$0.1(\epsilon_e/\epsilon_B)^{1/2}F_{\rm MeV}$ every decade for hours and days after the bursts. In this paper, when considering EGRET observations, we adopt 200 s after T_{90} (when electrons are in the fast-cooling regime) as the duration over which $F_{\rm GeV}$ is integrated.

3. CONSTRAINT ON HIGH-ENERGY EMISSION WITH EGRET

González Sánchez (2005) analyzed GRBs that were detected by BATSE and observed by EGRET. Since the field of view of EGRET was much smaller than that of BATSE and the observation was limited by the lifetime of the spark chamber, EGRET covered only about 100 GRBs out of $\sim$3000 BATSE bursts. However, this is still a reasonably large number for a statistically meaningful result. The analysis of the prompt burst in EGRET data was performed around the error circles of BATSE bursts for the first T_{90}, and a spectral index of -2.4 was assumed within the EGRET window (the upper limits are higher by a factor of $\approx$10 for a spectral index of -1). The same analysis was performed for the afterglow phase for 200 s after T_{90} (not including T_{90}). González Sánchez (2005) measured the fluence of 6 prompt phase and 12 afterglow phase GRBs. For all other GRBs, only fluence upper limits were obtained in the range 10^{-6}–10^{-3} erg cm^{-2}.

Here, we interpret these results in the framework of the SSC model, which implies that the fluences in the BATSE and EGRET bands are likely to be positively correlated through equation (1) ($F_{\rm BATSE} = F_{\rm MeV}$ and $F_{\rm EGRET} = F_{\rm GeV}$). We further assume that the coefficient η ($\eta_{\rm syn}$ for prompt and $\eta_{\rm IC}$ for afterglow phases) follows some probability distribution function $p(\eta)$ that is independent of $F_{\rm BATSE}$. We consider a lognormal distribution with a central value μ and a standard deviation σ:

$$p(\eta|\mu,\sigma)d\eta = \frac{1}{\sqrt{2\pi}\sigma}\exp\left[-\frac{(\log\eta-\mu)^2}{2\sigma^2}\right]d\log\eta. \quad (11)$$

Constraining μ and σ then leads to implications of GRB parameters such as ϵ_e, ϵ_B, and γ_m through the relations given in the previous section.

We used the observations to constrain μ and σ by carrying out a maximum-likelihood analysis.[4] Figure 2 shows the contour plot of the most likely region on the μ-σ plane for T_{90} (*left*) and for 200 s after T_{90} (*right*), assuming a spectral index of -2.4 (if the spectral index is -1, then μ increases by $\approx$1).

In that procedure, the detection efficiency of EGRET as a function of fluence, $\epsilon(F)$, is obtained from the distribution of the EGRET upper limits (for undetected GRBs), which is shown in Figure 3, i.e., a cumulative fraction of bursts whose fluence limits are below a given fluence. In the case of detected GRBs, on the other hand, the size of the error bars for the fluence is interpreted as the measurement accuracy of EGRET. Then, in order to test the consistency of the assumption that equation (11) fits the data, we carry out a Monte Carlo simulation that draws 10^5 realizations of EGRET observations, assuming that the distribution of $F_{\rm EGRET}/F_{\rm BATSE}$ follows equation (11) with the most likely values of μ and σ. By comparing the likelihood of these Monte Carlo realizations with that of the actual EGRET observations, we find that 70% of the realizations have a lower likelihood, suggesting that equation (11), with its most likely values, is indeed consistent with the observations.

[4] The log likelihood of a distribution is calculated by integrating the probability between the error bars and below the upper limits of the EGRET observations. For the T_{90} fluence data, we used the results of Fig. 2.3 of González Sánchez (2005) rather than her Tables 2.1 and 2.2.

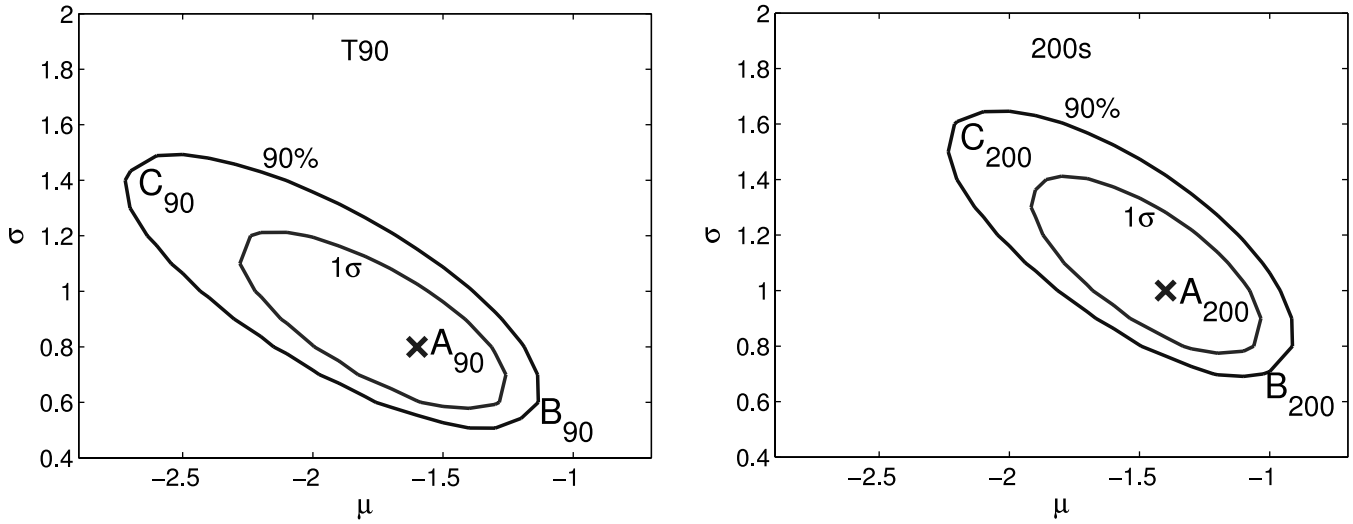

FIG. 2.—Contour plots of allowed region in μ-σ space, obtained with the analysis of EGRET data assuming a spectral index of -2.4, both during T_{90} (*left*) and 200 s after T_{90} (*right*). Here, μ and σ are the central value and standard deviation, respectively, for the lognormal distribution of the fluence ratio η (eq. [11]). The best-fit points (labeled "A") are marked as crosses, and other representative points (labeled "B" and "C") are also indicated in both panels. [*See the electronic edition of the Journal for a color version of this figure.*]

Given μ and σ, we can obtain the distribution of fluence in the EGRET band by convolving the BATSE fluence distribution ($dN/dF_{\rm BATSE}$; see Fig. 1) and $p(\eta|\mu,\sigma)$:

$$\frac{dN}{dF_{\rm EGRET}} = \int_0^\infty d\eta\, p(\eta|\mu,\sigma)\left|\frac{dN}{dF_{\rm BATSE}}\right|_{\eta^{-1}F_{\rm EGRET}}. \quad (12)$$

As representative models, we use three sets of (μ,σ) for both the prompt and afterglow cases. These are labeled as A_{T90}, B_{T90}, and C_{T90} (A_{200}, B_{200}, and C_{200}) and are shown in Figure 2. In Figure 4, we show the resulting fluence distribution corresponding to each of these models.

The EGRET results imply that during the prompt emission phase, $0.003 \lesssim \eta \lesssim 0.06$. As we discussed in § 2.1, the low number of photons in the bursts detected by EGRET, as well as their spectrum, implies that the detections of prompt photons are most likely to have been dominated by the high-energy tail of the synchrotron emission, i.e., that $\eta \approx \eta_{\rm syn}$ in Figure 2 (*left*). In fact, simply extrapolating the synchrotron tail of many BATSE bursts up to the $\sim$100 MeV regime using inferred values for $\nu_{\rm syn}$ and α_2 gives a value of $\eta_{\rm syn}$ consistent with the one obtained here for the prompt phase.

The harder IC prompt emission, however, can still have a fluence as much as 10 times larger than that of the synchrotron emission in the EGRET window without being detected. Therefore, this figure also sets an upper limit on the ratio of the IC and synchrotron components of $\eta_{\rm IC} \lesssim 0.6$, as a larger $\eta_{\rm IC}$ yields

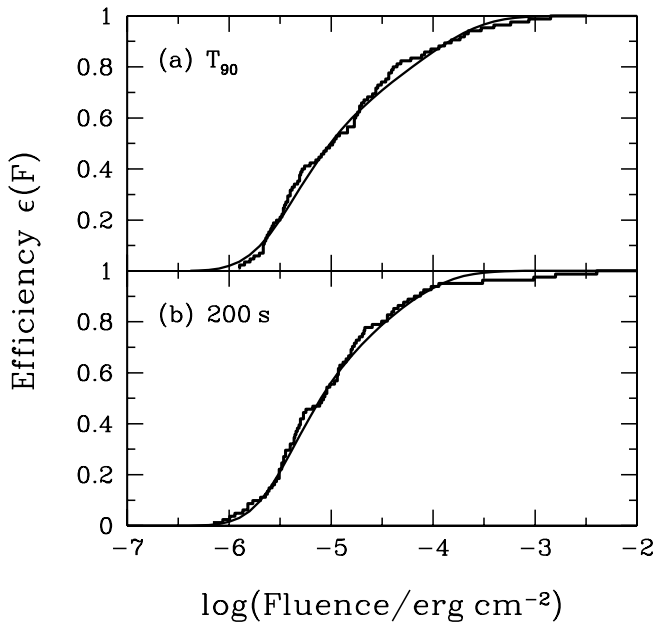

FIG. 3.—Efficiency of EGRET for GRBs as a function of fluence, $\epsilon(F)$, (*a*) during T_{90} and (*b*) 200 s after T_{90} (assuming a spectral index of -2.4). The histogram represents the cumulative fraction of GRBs whose fluence limits are below a given value, which can be interpreted as a detector efficiency, while the solid curves are a fitting function.

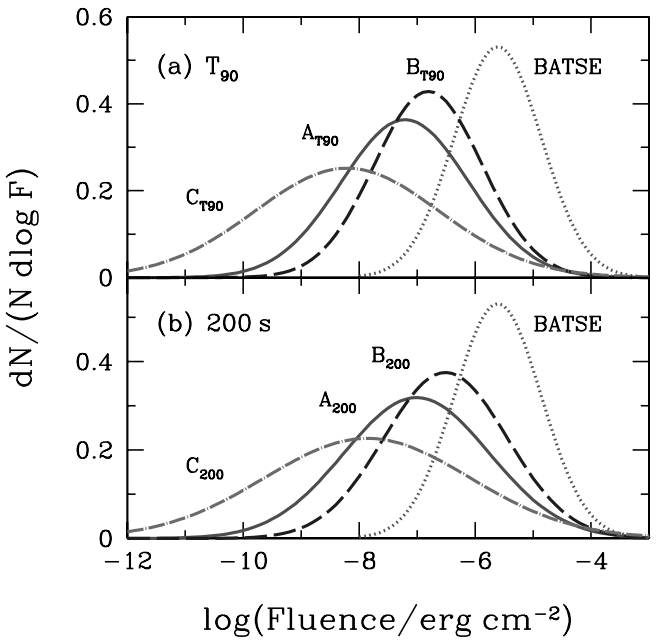

FIG. 4.—Distribution of EGRET fluences (*a*) during T_{90} and (*b*) 200 s after T_{90}. Models A–C correspond to the points on the μ-σ plots in Fig. 2. The BATSE fluence distribution is also plotted for comparison. The distribution for the prompt phase (*a*) is for the high-energy tail of the synchrotron radiation. The prompt IC fluence may be larger by up to about 1 order of magnitude (see text). [*See the electronic edition of the Journal for a color version of this figure.*]

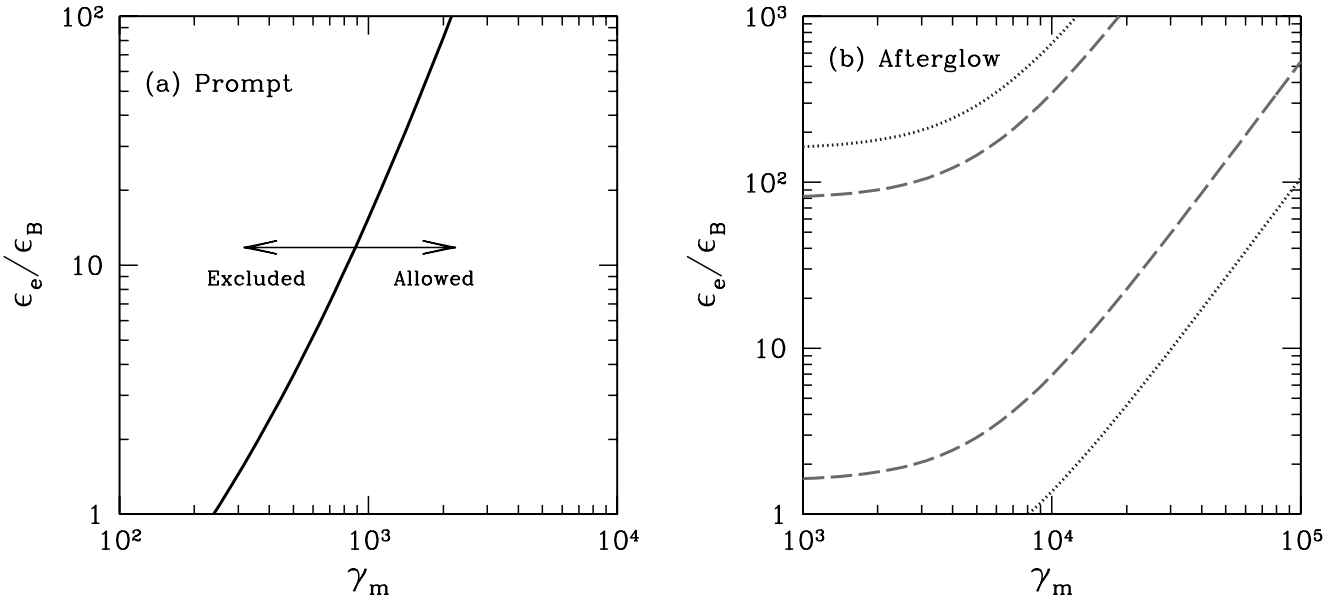

FIG. 5.—Illustrative constraint plot on ϵ_e/ϵ_B and γ_m from EGRET data for (*a*) prompt and (*b*) afterglow phases, obtained with canonical values for other parameters. The left and right regions of the solid curve in panel (*a*) represent excluded and allowed regions, respectively, while the regions between the two dashed (dotted) curves in panel (*b*) show allowed regions corresponding to $0.013 < \eta_{\rm IC} < 0.09$ ($0.006 < \eta_{\rm IC} < 0.13$). Note, however, that these regions could easily change depending on the values of other parameters. [*See the electronic edition of the Journal for a color version of this figure.*]

enough photon fluence to be detectable by EGRET. As we showed in § 2.1, we theoretically predict $\eta_{\rm IC} \approx 1.2$ (for EGRET) with a canonical set of parameters. Although this appears to imply that the current bound from EGRET already excludes the canonical model, we cannot make such a strong statement given the current uncertainties of many relevant parameters. Therefore, a more conservative statement would be that the current EGRET bound is barely consistent with the predictions of the SSC within the internal shock model. We may interpret the bound $\eta_{\rm IC} \lesssim 0.6$ as a constraint on ϵ_e/ϵ_B and γ_m, which is shown in Figure 5*a*. As the Klein-Nishina suppression ($\xi_{\rm KN}$) becomes significant for large γ_m, we have only a modest limit on ϵ_e/ϵ_B in such a regime. However, one should keep in mind that these are order-of-magnitude constraints, which may vary further with other parameters such as $\nu_{\rm syn}$, α_2, and Γ_b. A much better constraint plot is expected with the future *GLAST* data, where it is hoped that $\eta_{\rm IC}$ will be measured for many individual bursts.

During the afterglow, the synchrotron emission is much softer than it is during the prompt phase, and therefore the IC component is also expected to dominate EGRET observations near its lower energy band limit. Moreover, the fact that the number of bursts detected by EGRET during the afterglow is higher than the number detected during the prompt emission phase suggests that here EGRET is likely to have detected the actual IC component of the afterglow. The spectral index of the GeV afterglow in the EGRET window during the first 200 s is expected to be $\alpha = 1.5$–2, implying that the evaluation of μ in the right panel of Figure 2, which assumes a spectral index of -2.4, might be larger by at most a small factor ($\sim$2–3). Thus, for the afterglow, $\eta_{\rm IC} \sim 0.01$–0.1. We then compare this result with the theoretical expectation of $\eta_{\rm IC}$ in equation (2). First, however, we need to estimate the value of $F_{\rm syn}/F_{\rm MeV}$, where $F_{\rm syn}$ is measured during the first 200 s following T_{90}, and $F_{\rm MeV}$ is the prompt emission fluence. We use the *Swift* GRB table,[5] which provides X-ray afterglow fluences several tens to several hundreds of seconds after the bursts, as well as the prompt MeV fluences. Using only bursts for which the X-ray observation starts after T_{90} but no more than 300 s after the burst, we find a distribution of $F_{\rm syn}/F_{\rm MeV}$ that ranges from 10^{-3} to 0.1, with a central value of $\sim 10^{-2}$. Thus, afterglow theory with canonical parameters predicts $\eta_{\rm IC} \sim 10^{-2}$ with a large spread, which is consistent with the EGRET constraints. Figure 5*b* shows the interpretation of the EGRET constraints on $\eta_{\rm IC}$ (Fig. 2) as a function of ϵ_e/ϵ_B and γ_m, assuming canonical parameters and $F_{\rm syn}/F_{\rm MeV} = 10^{-2}$. Although this allowed region may change with other model parameters, again one cannot have too large a value of γ_m because of the Klein-Nishina suppression factor $\xi_{\rm KN}$.

4. IMPLICATION FOR *GLAST*

We now move on to discussions of the implications for *GLAST* using the constraints on η obtained in the previous section. First, we estimate the sensitivity of the LAT on board *GLAST* for prompt and afterglow GeV emission based on its published sensitivity to steady point sources,[6] which is 4×10^{-9} cm^{-2} s^{-1} above 100 MeV at 5 σ, with a power-law index of -2. This sensitivity was obtained by a one-year all-sky survey during which any point source was observed for $\sim$70 days (the LAT field of view is 2.4 sr).[7] Therefore, during the background-limited regime (when t is large enough that many background photons can be observed), the flux limit scales with t as 4×10^{-9} cm^{-2} s^{-1} (t/70 days)$^{-1/2}$. During the photon-count-limited regime (when t is so small that less than 1 background photon is expected), on the other hand, the detection limit is at a constant fluence. Therefore, the fluence sensitivity of the *GLAST* LAT detector is

$$F_{\rm lim}(t) \approx \begin{cases} F_{\rm lim}(t_0) & \text{for } t \le t_0, \\ F_{\rm lim}(t_0)\left(\dfrac{t}{t_0}\right)^{1/2} & \text{for } t > t_0, \end{cases} \tag{13}$$

[5] See http://swift.gsfc.nasa.gov/docs/swift/archive/grb_table/.

[6] See http://www-glast.slac.stanford.edu/.

[7] We assume here a step function for the LAT window function.

TABLE 1
GLAST LAT Fluence Sensitivity

α	t_0 (s)	$F_{\rm lim}(t \le t_0)$ (erg cm^{-2})	$F_{\rm lim}(10^3$ s) (erg cm^{-2})
2.3.....	650	4.5×10^{-7}	5.6×10^{-7}
2.0.....	650	6.6×10^{-7}	8.1×10^{-7}
1.0[a]	650	5.2×10^{-6}	6.4×10^{-6}

Note.—Parameters of point-source fluence sensitivity (integrated over 30 MeV–30 GeV) of *GLAST* LAT (see eq. [13]). The power-law index is $-\alpha$, and the fluence limit $F_{\rm lim}$ is in units of erg cm^{-2}. The detection criterion for $t \le t_0$ is five photons, and significance for $t > t_0$ is 5 σ, where $t_0 = 650$ s is the transition time.

[a] Here we considered a detection based on the number of photons in the energy range 30 MeV–30 GeV. A higher t_0 and a more sensitive background-limited threshold can be obtained for $\alpha = 1$ if a higher energy range is considered (see text and Appendix B).

TABLE 2
GRB Rate at *GLAST* LAT and Contribution to the EGB Flux

Model	Rate at *GLAST* (yr^{-1})	$I_{\rm EGB}$ (GeV cm^{-2} s^{-1} sr^{-1})
Prompt Phase (during T_{90})		
A_{T90}	15	$6.3\times10^{-10}(1+\eta_{\rm IC}/\eta_{\rm syn})$
B_{T90}	20	$8.4\times10^{-10}(1+\eta_{\rm IC}/\eta_{\rm syn})$
C_{T90}	10	$4.4\times10^{-10}(1+\eta_{\rm IC}/\eta_{\rm syn})$
Afterglow Phase (200 s after T_{90})		
A_{200}	20	8.9×10^{-10}
B_{200}	30	1.3×10^{-9}
C_{200}	15	6.5×10^{-10}

Note.—The table displays the estimate of detection rate with *GLAST* LAT (for $\alpha = 2.3$) and expected EGB intensity for models A, B, and C of the prompt (during T_{90}) and afterglow phases (200 s after T_{90}). The correction factor $1 + \eta_{\rm IC}/\eta_{\rm syn}$ for $I_{\rm EGB}$ in the case of prompt emission could be as large as $\sim$10. Also note that these estimates are quite conservative. See discussions in §§ 4 and 5 for more details.

where $t_0 = 650$ s represents the time when the transition from the photon-count-limited to the background-limited regime occurs in the LAT case. Note that equation (13) is for the limiting *fluence*, the time-integrated flux, rather than for the flux. This limit is more natural in the photon-count-limited regime, and it is more relevant to the EGRET constraints that we derived in the previous section. Detailed derivation of this sensitivity is given in Appendix B. In Table 1, we summarize the values of t_0 and $F_{\rm lim}(t)$ for a few cases of power-law index $-\alpha$ and integration time t. The values of $F_{\rm lim}(t)$ for $t \ll t_0$ in the table are determined by a criterion of five-photon detection, while those for $t > t_0$ are determined by 5 σ significance. The fluence we argue here is the one integrated over 30 MeV–30 GeV, in order to compare with the EGRET fluence upper bounds.

In the case of the background-limited regime, it might be more appropriate to use a higher energy threshold (instead of 30 MeV), especially for the hard source spectrum, because the background spectrum falls steeply with frequency ($\alpha \simeq 2.1$). Depending on the spectral index of the GRB emissions, we may be able to find the optimal low-frequency threshold; the threshold is higher for a harder spectrum. Thus, we should be able to improve the fluence sensitivity for the background-limited regime over the figures given in Table 1. In addition, the transition from the photon-count-limited to the background-limited regime would occur later than 650 s. For our purpose, however, since the timescales we consider (T_{90} for prompt emission and 200 s after T_{90} for afterglows) are both during the photon-count-limited regime, the above consideration does not apply, and we can use the full energy range (30 MeV–30 GeV for EGRET) to collect as many photons as possible.

GLAST is also equipped with the *GLAST* Burst Monitor (GBM) instrument, which is dedicated to the detection of GRBs. It detects photons of 8 keV to more than 25 MeV, and its field of view is $\sim$8 sr. The expected rate of GRBs that trigger the GBM is $\sim$200 yr^{-1} (McEnery & Ritz 2006), which is almost as high as the BATSE rate. Each year, about 70 out of these $\sim$200 bursts should fall within the LAT field of view. Given the distribution of fluences (Fig. 4) and the LAT sensitivity (Table 1), we can estimate the fraction of GRBs that would be detected with the LAT. In Table 2, we show the expected LAT detection rate for $\alpha = 2.3$, which is $\sim$20 yr^{-1} for the best-fit models of the EGRET data for both the prompt and afterglow emissions. The prompt phase estimates are for detections of the synchrotron component in the $\sim$100 MeV range. Given the large effective area of the LAT, it is also expected to detect $\gtrsim$GeV photons from the IC component and to identify the spectral break associated with the transition from the synchrotron to the IC component, thereby directly testing the SSC model.

The estimates given in Table 2 are fairly conservative. First, although we used a five-photon criterion for the detection, even a two-photon detection should be quite significant, because the expected background count is much smaller than one photon during T_{90} and the following 200 s that we considered. Second, *Swift* can find dimmer bursts than the GBM can. Although the discovery rate is not as high as that of the GBM or BATSE, it would still be able to find tens of new GRBs in the LAT field of view. Thus, the true rate would likely be larger than the figures given in Table 2.

5. IMPLICATION FOR THE EXTRAGALACTIC GAMMA-RAY BACKGROUND

All the GRBs except for those detected by EGRET should contribute to the EGB flux to a certain extent (Dermer 2007). This may be computed as

$$I_{\rm EGB} = \frac{R_{\rm GRB}}{4\pi}\int_0^\infty dF\, F\frac{dP}{dF}[1-\epsilon(F)], \qquad (14)$$

where F is EGRET fluence in the 30 MeV–30 GeV range, dP/dF is the normalized distribution of EGRET fluence (eq. [12] and Fig. 4), and $R_{\rm GRB} \sim 2$ day^{-1} is the occurrence rate of GRBs over the entire sky. The factor $1 - \epsilon(F)$ takes into account the fact that very bright GRBs cannot contribute to the EGB because they would be identified as point sources (but see discussions below). Figure 6 shows the differential EGB intensity $dI_{\rm EGB}/d\log F$, which represents contributions from GRBs of a given fluence for the prompt and afterglow phases. In the third column of Table 2, we show the EGB intensity due to the prompt and afterglow phases of GRBs, which is $\sim10^{-9}$ GeV cm^{-2} s^{-1} sr^{-1}. On the other hand, in the same energy range, EGRET measured the EGB flux to be 10^{-5} GeV cm^{-2} s^{-1} sr^{-1} (Sreekumar et al. 1998). Therefore, GRBs that were detected by BATSE but not detected as point sources by EGRET contribute at least $\sim$0.01% to the EGB. Again, we note that the estimates for the prompt phase are those of the synchrotron component. We thus need to take the predicted IC contribution into account, which is represented by a correction factor $1 + \eta_{\rm IC}/\eta_{\rm syn}$ in Table 2. Since this factor could be as large as $\sim$10 according to the discussion in § 3, EGB flux due to the prompt phase of GRBs could also become $\sim$10 times larger,

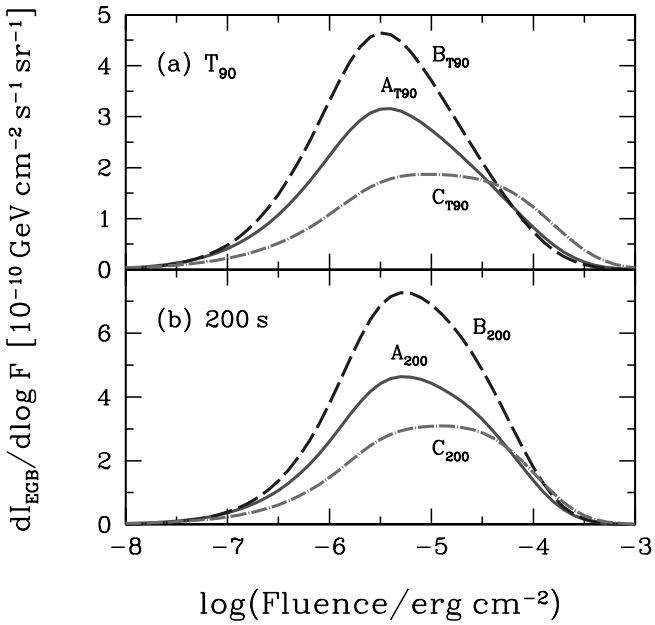

FIG. 6.—Contribution to the EGB intensity $I_{\rm EGB}$ from GRBs of given fluence, for (*a*) prompt (during T_{90}) and (*b*) afterglow (200 s after T_{90}) emission phases. In each panel, three models A–C are shown. Note that for the prompt phase, the fluence is that for synchrotron radiation, and that for the IC component could be even larger (see text). [*See the electronic edition of the Journal for a color version of this figure.*]

making the GRB contribution as large as ~0.1% of the observations above ~1 GeV. In any case, the contributions from other astrophysical sources such as blazars are expected to be more significant than GRBs (e.g., Ando et al. 2007 and references therein).

Additional contributions to EGBs are expected from a large number of GRBs that point away from us, and therefore would not have been detected with BATSE. The emission from these bursts points toward us once the external shock decelerates (Rhoads 1997). Since the total GeV energy emitted during every decade of the afterglow is roughly constant, the contribution of these GRBs to the EGB can be estimated by the GeV emission of the bursts that were detected by BATSE. Similar contributions are expected from bursts that point toward us but that are too faint to be detected by BATSE, if the GRB luminosity function behaves as $\phi(L) \propto L^{-2}$ as suggested by the universal structured jet model (Lipunov et al. 2001; Rossi et al. 2002; Zhang & Mészáros 2002; Perna et al. 2003; see, however, Guetta et al. 2005). Therefore, the contribution to the EGB of bursts that were not detected by BATSE can be estimated by the afterglow fluence of the detected bursts, assuming no contribution from bursts with only an upper limit. This is a reasonable estimate, since the GeV flux is dominated by the few brightest bursts in GeV, which are the most likely to be detected. Taking the fluence of the detected GeV bursts as the logarithmic mean of these upper and lower limits implies $I_{\rm EGB} \sim 5 \times 10^{-9}$ GeV cm^{-2} s^{-1} sr^{-1}, making the GRB contribution ~0.1% of the EGB.

Finally, we note that there is a large uncertainty in removing the Galactic foreground contamination from the total diffuse flux (Keshet et al. 2004). In addition, EGRET observations do not constrain TeV emission that cascades down into the GeV range for GRBs at cosmological distances (Casanova et al. 2007; Murase et al. 2007). Thus, if the foreground subtraction has indeed been underestimated or if the GRB TeV emission is not negligible, then the GRB contribution might be much more significant than the estimates here.

6. SUMMARY AND CONCLUSIONS

The *GLAST* satellite would enable us to test high-energy emission mechanisms of GRBs. If this emission is found to be consistent with SSC, then its observations would constrain physical parameters such as the ϵ_e/ϵ_B ratio and the bulk Lorentz factor of the jet, Γ_b. The EGRET instrument on board *CGRO*, while less sensitive than the *GLAST* LAT detector, has identified several BATSE GRBs with GeV photons. In addition, stringent upper limits for ~100 GRBs were set on fluences in the GeV band by analyzing the EGRET data (González Sánchez 2005).

In this paper, we further extended this EGRET result, comparing it with the SSC emission model. Following theoretical models of SSC emission, we assumed that there is a linear correlation between fluences in the BATSE and EGRET energy bands, and that the proportionality coefficient η follows a lognormal distribution. We found that the predictions from the SSC model using canonical parameter values are fully consistent with EGRET fluence measurements and upper limits for both the prompt and afterglow phases. During the course of showing this result, we properly took the Klein-Nishina feedback effect into account in the theoretical calculation. The best-fit value of the coefficient was $\log \eta \simeq -1.5$ for both the prompt and afterglow emissions, and it is already stringent enough to test the SSC scenario. The limits for the prompt emission phase are for synchrotron radiation, and thus if we consider the IC component as well, the value of η could be larger by up to 1 order of magnitude.

The obtained η distribution, together with the BATSE fluence distribution, gives the expected fluence distribution in the GeV band, which is shown in Figure 4. As the *GLAST* LAT detector covers the EGRET energy band, we can predict the number of GRBs detectable with *GLAST* from the distribution of $F_{\rm EGRET}$, given the *GLAST* LAT sensitivity. Our conservative estimate using the five-photon criterion is that about ~20 GRBs of those detected with the GBM would be detected with *GLAST* LAT each year. This number could be even larger if we use a fewer-photon criterion. The fluence distribution can also be used to estimate the GRB contribution to the EGB intensity. We found that the contribution would be at least ~0.01%, but that it is likely to be as large as ~0.1%.

We are grateful to B. L. Dingus and M. M. González Sánchez for very helpful comments and discussions. We thank the referee for useful comments. This work was supported by the Sherman Fairchild Foundation (S. A. and E. N.), a NASA Swift Grant (E. N.), the Alfred P. Sloan Foundation, the Packard Foundation, and a NASA ATP Grant (R. S.).

APPENDIX A

KLEIN-NISHINA FEEDBACK ON HIGH-ENERGY EMISSION

We find an analytic expression for $\xi_{\rm KN}$ due to the Klein-Nishina feedback. To simplify the argument such that we can treat it analytically, we make the following approximations: (1) an electron with a fixed Lorentz factor γ_e radiates monoenergetic synchrotron photons; (2) the same electron upscatters a given synchrotron photon to another monochromatic energy, which is increased by a factor of

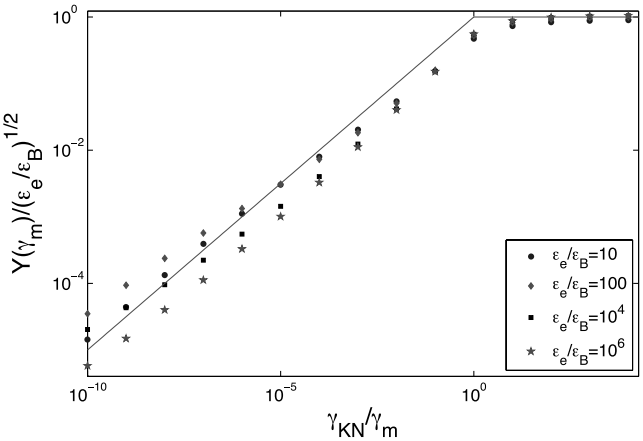

FIG. 7.—Ratio of IC to synchrotron power Y by an electron with Lorentz factor γ_m as a function of $\gamma_{\rm KN}/\gamma_m$. Points represent numerical solutions of eq. (A1) for various values of ϵ_e/ϵ_B, while the solid line is an analytic fit (eq. [5]). [*See the electronic edition of the Journal for a color version of this figure.*]

γ_e^2; (3) νf_ν of the synchrotron and IC photons peaks at $\nu_{\rm syn}$ (a synchrotron frequency corresponding to γ_m) and $\nu_{\rm IC}$ ($=\gamma_m^2\nu_{\rm syn}$ if there is no Klein-Nishina suppression), respectively; (4) the Klein-Nishina cutoff occurs quite sharply above its threshold; (5) both cooling and self-absorption frequencies are much smaller than the frequency region of our interest; and (6) electrons cool so quickly that any dynamical effects can be neglected. With these approximations, the expression for the ratio of the power of the synchrotron and IC radiation from a given electron $Y(\gamma_e) = P_{\rm IC}(\gamma_e)/P_{\rm syn}(\gamma_e)$ is simplified significantly. In particular, according to assumption (3) above, we have $(\epsilon_e/\epsilon_B)^{1/2}\xi_{\rm KN} \approx Y(\gamma_m)$. This is given as

$$Y(\gamma_m) = \frac{\epsilon_e}{\epsilon_B}\frac{p/2-1}{p-1}(\nu'_{\rm syn})^{p/2-1}\int_0^\infty d\nu'\,\frac{\max(\nu',\nu'_{\rm syn})^{-(p-1)/2}(\nu')^{-1/2}}{1+Y\left([\nu'/\nu'_{\rm syn}]^{1/2}\gamma_m\right)}\Theta\left(-\nu'+\frac{m_ec^2}{h\gamma_m}\right), \tag{A1}$$

where p is the electron spectral index, Θ is the step function, and primed quantities are evaluated in the rest frame of the ejecta (e.g., $\nu' = \nu/\Gamma_b$, where ν is the frequency in the observer's frame).

A detailed derivation and numerical approaches will be given elsewhere (E. Nakar et al., in preparation), but at least this equation can be understood qualitatively. For a given electron with a Lorentz factor γ_m, the synchrotron power does not depend on whether the Klein-Nishina suppression is effective or not. On the other hand, the IC power does, because it is proportional to the energy density of the seed (synchrotron) photons integrated up to some cutoff frequency; synchrotron photons above this frequency cannot be IC scattered efficiently by the electron with γ_m because of Klein-Nishina suppression. The integrand of equation (A1) represents the synchrotron spectrum. More specifically, assuming no Klein-Nishina suppression, the spectrum is simply given by $f_{\nu'} \propto \max[\nu',\nu'_{\rm syn}]^{-(p-1)/2}(\nu')^{-1/2}$; the step function then represents the Klein-Nishina cutoff. The factor $1+Y$ in the denominator of the integrand accounts for the suppression of the electron distribution function due to the enhanced IC cooling; i.e., $dN_e/d\gamma_e \propto (d\gamma_e/dt)^{-1} \propto [P_{\rm syn}(\gamma_e)+P_{\rm IC}(\gamma_e)]^{-1} \propto [1+Y(\gamma_e)]^{-1}$. These electrons are ones that emit synchrotron photons of a given frequency ν'. Recalling the relation $\gamma_e \propto \nu'^{1/2}$, their Lorentz factor is given by $(\nu'/\nu'_{\rm syn})^{1/2}\gamma_m$, which appears in the argument of Y in the integrand. Finally, the other constants in equation (A1) are chosen so that we have a proper relation for the fast-cooling regime, $Y(1+Y) = \epsilon_e/\epsilon_B$, if we turn off the Klein-Nishina cutoff and have constant Y.

We now find analytic expressions of equation (A1) in asymptotic regions. We start from the case of $\gamma_m \lesssim \gamma_{\rm KN} = m_ec^2/h\nu'_{\rm syn}$, which is equivalent to $\nu'_{\rm syn} < m_ec^2/h\gamma_m$. The integration then becomes

$$Y(\gamma_m) = \frac{\epsilon_e}{\epsilon_B}\frac{p/2-1}{p-1}\left[\int_0^{\nu'_{\rm syn}} d\nu'\,\frac{(\nu'_{\rm syn}\nu')^{-1/2}}{1+Y\left((\nu'/\nu'_{\rm syn})^{1/2}\gamma_m\right)} + \int_{\nu'_{\rm syn}}^{m_ec^2/h\gamma_m} d\nu'\,\frac{(\nu'_{\rm syn})^{p/2-1}(\nu')^{-p/2}}{1+Y\left((\nu'/\nu'_{\rm syn})^{1/2}\gamma_m\right)}\right]. \tag{A2}$$

We assume that the function $1+Y$ varies rather mildly in the integrand, so that in the argument of Y we may use $\nu' = \nu'_{\rm syn}$. Then the integral can be evaluated analytically, which gives $Y(\gamma_m)[1+Y(\gamma_m)] = \epsilon_e/\epsilon_B$. When $\epsilon_e \gg \epsilon_B$, we have $Y(\gamma_m) = (\epsilon_e/\epsilon_B)^{1/2}$, which is the same result as in the case of no Klein-Nishina suppression. This makes sense, because the condition $\gamma_m < \gamma_{\rm KN}$ indicates that electrons with γ_m are below the Klein-Nishina threshold, with seed photons at frequency $\nu'_{\rm syn}$ dominating the synchrotron power. On the other hand, when $\gamma_m > \gamma_{\rm KN}$ (or $\nu'_{\rm syn} > m_ec^2/h\gamma_m$), equation (A1) becomes

$$Y(\gamma_m) = \frac{\epsilon_e}{\epsilon_B}\frac{p/2-1}{p-1}\int_0^{m_ec^2/h\gamma_m} d\nu'\,\frac{(\nu'_{\rm syn}\nu')^{-1/2}}{1+Y\left([\nu'/\nu'_{\rm syn}]^{1/2}\gamma_m\right)} \approx \frac{\epsilon_e}{\epsilon_B}\frac{p-2}{p-1}\left(\frac{\gamma_m}{\gamma_{\rm KN}}\right)^{-1/2}\frac{1}{1+Y\left([\gamma_m\gamma_{\rm KN}]^{1/2}\right)}, \tag{A3}$$

where in the second equality we use $\nu' = m_ec^2/h\gamma_m$ for the argument of Y. When $\gamma_m/\gamma_{\rm KN}$ is sufficiently large that $Y([\gamma_m\gamma_{\rm KN}]^{1/2}) \ll 1$, then equation (A3) immediately gives an asymptotic solution for $Y(\gamma_m)$. When γ_m is in the intermediate regime, we can still get analytic expressions; however, these are given elsewhere because they are somewhat complicated. Here we simply show numerical solutions of equation (A1) as a function of $\gamma_{\rm KN}/\gamma_m$ for various values of ϵ_e/ϵ_B. We show these results, as well as a simple fitting form (given by eq. [5]), in Figure 7. Thus, equation (5) provides a fairly good fit to the results of numerical integration of equation (A1).

APPENDIX B

FLUENCE SENSITIVITY OF *GLAST*

For a steady point source with a spectral index of -2, the sensitivity of *GLAST* LAT to its flux above 100 MeV is 4×10^{-9} cm^{-2} s^{-1} at 5 σ significance for a one-year all-sky survey. Considering the 2.4 sr field of view of *GLAST* LAT, this survey time corresponds to 70 days of exposure time to the source; therefore, the sensitivity to the number fluence integrated over this timescale is 2.4×10^{-2} cm^{-2}. In this section, we generalize this limit to an arbitrary spectral index $-\alpha$ and exposure time t.

Before starting the discussion, we define the differential number and energy fluences, and the integrated number and energy fluences (all quantities are time integrated):

$$\frac{dF_N}{dE} = CE^{-\alpha}, \quad \frac{dF}{dE} = CE^{1-\alpha}, \tag{B1}$$

$$F_N = C\frac{E_{\rm max}^{1-\alpha} - E_{\rm min}^{1-\alpha}}{1-\alpha}, \quad F = C\frac{E_{\rm max}^{2-\alpha} - E_{\rm min}^{2-\alpha}}{2-\alpha}, \tag{B2}$$

where C is a coefficient, and $E_{\rm min}$ and $E_{\rm max}$ are the energy band boundaries.

The fluence sensitivity for a 1 yr exposure is within the background-limited regime; namely, within 1 yr many background photons are expected to be detected within the point-spread function of the detector. In the case of *GLAST* LAT, backgrounds are the EGB or Galactic foreground emissions. Therefore, we start our discussion from this background-limited case. Let us define this background rate of *GLAST* as $\dot{N}_{\rm bg}$, for which we assume an $E^{-2.1}$ spectrum and use the energy-dependent angular resolution and on-source effective area $A_{\rm eff}(E)$.[8] The criterion of point-source detection is

$$N_\gamma > N_{\gamma,\,\rm lim} \equiv \sigma\sqrt{\dot{N}_{\rm bg} t}, \tag{B3}$$

where σ represents the significance of detection, and the photon count from the source is obtained by

$$N_\gamma = \int_{E_{\rm min}}^{E_{\rm max}} dE\, \frac{dF_N}{dE} A_{\rm eff}(E). \tag{B4}$$

Therefore, using equation (B1) in equations (B4) and (B3), we can obtain the sensitivity to the coefficient $C_{\rm lim}$ as follows:

$$C_{\rm lim} = N_{\gamma,\,\rm lim}\left[\int_{E_{\rm min}}^{E_{\rm max}} dE\, E^{-\alpha} A_{\rm eff}(E)\right]^{-1}, \tag{B5}$$

and then using equation (B2); this can be translated into the sensitivity to the number and energy fluences, $F_{N,\,\rm lim}$ and $F_{\rm lim}$. We note here that $C_{\rm lim}$ depends on t, α, $E_{\rm min}$, and $E_{\rm max}$, while $N_{\gamma,\rm lim}$ depends only on t, $E_{\rm min}$, and $E_{\rm max}$. In this background-limited regime, the time dependence is $F_{\rm lim} \propto t^{1/2}$, from equation (B3). We have confirmed, using the EGB intensity measured by EGRET (Sreekumar et al. 1998) and the energy-dependent angular resolution of the LAT, that we could obtain the limit comparable to $F_{N,\,\rm lim} = 2.4 \times 10^{-2}$ cm^{-2} for the case of $\alpha = 2$, $t = 70$ days, $E_{\rm min} = 100$ MeV, $E_{\rm max} = \infty$, and $\sigma = 5$. The results of this procedure for several values of interest of α are summarized in equation (13) and Table 1. Here, we used the EGRET energy range, i.e., $E_{\rm min} = 30$ MeV and $E_{\rm max} = 30$ GeV, but we could adopt different values.

If the timescale is short, such that $N_{\gamma,\,\rm lim} < 1$, then the argument above does not apply; rather the sensitivity is simply obtained by the expected photon count from the source. In this photon-count-limited regime, we can evaluate the fluence sensitivity by requiring N_γ to be a few; here, we use $N_\gamma = 5$. One can obtain the corresponding $C_{\rm lim}$ by solving this criterion using equation (B4). This time, $C_{\rm lim}$ is independent of t. Then again, using equation (B2), one can get the fluence sensitivity in this regime as shown in Table 1.

[8] For these specifications of the detector, we use the results from http://www-glast.stanford.edu/.

REFERENCES

Ando, S. 2004, MNRAS, 354, 414
Ando, S., Komatsu, E., Narumoto, T., & Totani, T. 2007, Phys. Rev. D, 75, 063519
Asano, K., & Inoue, S. 2007, ApJ, 671, 645
Band, D., et al. 1993, ApJ, 413, 281
Baring, M. G., & Harding, A. K. 1997, ApJ, 491, 663
Casanova, S., Dingus, B. L., & Zhang, B. 2007, ApJ, 656, 306
Chiang, J., & Dermer, C. D. 1999, ApJ, 512, 699
Derishev, E. V., Kocharovsky, V. V., Kocharovsky, V. V., & Mészáros, P. 2003, in AIP Conf. Proc. 662, Gamma-Ray Burst and Afterglow Astronomy 2001: A Workshop Celebrating the First Year of the HETE Mission, ed. G. R. Ricker & R. K. Vanderspek (Melville: AIP), 292
Dermer, C. D. 2007, in AIP Conf. Proc. 921, The First *GLAST* Symposium, ed. S. Ritz, P. Michelson, & C. A. Meegan (Melville: AIP), 122
Dermer, C. D., Chiang, J., & Mitman, K. E. 2000, ApJ, 537, 785
Fan, Y.-Z., Piran, T., Narayan, R., & Wei, D.-M. 2008, MNRAS, 384, 1483
González Sánchez, M. M. 2005, Ph.D. thesis, Univ. Wisconsin, Madison
González Sánchez, M. M., Dingus, B. L., Kaneko, Y., Preece, R. D., Dermer, C. D., & Briggs, M. S. 2003, Nature, 424, 749
Gou, L.-J., & Mészáros, P. 2007, ApJ, 668, 392
Granot, J., Cohen-Tanugi, J., & do Cauto e Silva, E. 2008, ApJ, 677, 92
Guetta, D., & Granot, J. 2003, ApJ, 585, 885
Guetta, D., Piran, T., & Waxman, E. 2005, ApJ, 619, 412
Hurley, K., et al. 1994, Nature, 372, 652
Ioka, K., Murase, K., Toma, K., Nagataki, S., & Nakamura, T. 2007, ApJ, 670, L77
Kaneko, Y., Preece, R. D., Briggs, M. S., Paciesas, W. S., Meegan, C. A., & Band, D. L. 2006, ApJS, 166, 298

Keshet, U., Waxman, E., & Loeb, A. 2004, J. Cosmol. Astropart. Phys., 04, 006
Lipunov, V. M., Postnov, K. A., & Prokhorov, M. E. 2001, Astron. Rep., 45, 236
Lithwick, Y., & Sari, R. 2001, ApJ, 555, 540
McEnery, J., & Ritz, S. 2006, in AIP Conf. Proc. 836, Gamma-Ray Bursts in the Swift Era, ed. S. S. Holt, N. Gehrels, & J. A. Nousek (Melville: AIP), 660
Medvedev, M. V. 2000, ApJ, 540, 704
Mészáros, P. 2006, Rep. Prog. Phys., 69, 2259
Mészáros, P., Rees, M. J., & Papathanassiou, H. 1994, ApJ, 432, 181
Moderski, R., Sikora, M., Coppi, P. S., & Aharonian, F. 2005a, MNRAS, 363, 954
———. 2005b, MNRAS, 364, 1488
Murase, K., Asano, K., & Nagataki, S. 2007, ApJ, 671, 1886
Murase, K., & Ioka, K. 2008, ApJ, 676, 1123
Nakar, E. 2007, Phys. Rep., 442, 166
Panaitescu, A. 2008, MNRAS, 385, 1628
Panaitescu, A., & Kumar, P. 2000, ApJ, 543, 66
———. 2001, ApJ, 560, L49
Pe'er, A., & Waxman, E. 2004, ApJ, 613, 448
———. 2005, ApJ, 633, 1018
Perna, R., Sari, R., & Frail, D. 2003, ApJ, 594, 379
Piran, T. 1999, Phys. Rep., 314, 575
———. 2005, Rev. Mod. Phys., 76, 1143
Preece, R. D., Briggs, M. S., Mallozzi, R. S., Pendleton, G. N., Paciesas, W. S., & Band, D. L. 2000, ApJS, 126, 19
Razzaque, S., Mészáros, P., & Zhang, B. 2004, ApJ, 613, 1072
Rhoads, J. E. 1997, ApJ, 487, L1
Rossi, E., Lazzati, D., & Rees, M. J. 2002, MNRAS, 332, 945
Rybicki, G. B., & Lightman, A. P. 1979, Radiative Processes in Astrophysics (New York: Wiley-Interscience)
Sari, R., & Esin, A. A. 2001, ApJ, 548, 787
Schneid, E. J., et al. 1992, A&A, 255, L13
———, et al. 1995, ApJ, 453, 95
Sommer, M., et al. 1994, ApJ, 422, L63
Sreekumar, P., et al. 1998, ApJ, 494, 523
Strong, A. W., Moskalenko, I. V., & Reimer, O. 2004, ApJ, 613, 956
Waxman, E. 1997, ApJ, 485, L5
Wei, D. M., & Lu, T. 1998, ApJ, 505, 252
Yost, S. A., Harrison, F. A., Sari, R., & Frail, D. A. 2003, ApJ, 597, 459
Zhang, B., & Mészáros, P. 2001, ApJ, 559, 110
———, P. 2002, ApJ, 571, 876